Structure of the Mn Complex in Photosystem II:

Insights from X-ray Spectroscopy

Vittal K. Yachandra

Melvin Calvin Laboratory, Physical Biosciences Division,

Lawrence Berkeley National Laboratory, Berkeley, CA 94720

Abstract

We have used Mn K-edge absorption and Kβ emission spectroscopies to determine the oxidation states of the Mn complex in the various S-states. We have started exploring the new technique of resonant inelastic X-ray scattering spectroscopy (RIXS); this technique can be characterized as a Raman process that uses K-edge energies (1s to 4p, ~6550 eV) to obtain L-edge-like spectra (2p to 3d, ~650 eV). The relevance of these data to the oxidation states and structure of the Mn complex is presented. We have obtained EXAFS data from the S_0 and S_3 states and observed heterogeneity in the Mn-Mn distances, leading us to conclude that there may be three rather than two di-μ-oxo bridged units present per tetranuclear Mn cluster. In addition, we have obtained data using Ca/Sr X-ray spectroscopy that provide evidence for a heteronuclear Mn/Ca cluster. The possibility of three di-μ-oxo-bridged Mn–Mn moieties and the proximity of Ca is incorporated into developing structural models for the Mn cluster. The involvement of bridging and terminal O ligands of Mn in the mechanism of oxygen evolution is discussed in the context of our X-ray spectroscopy results.

1. **Introduction**

Critical questions related to the process of photosynthetic water oxidation catalyzed by a Mn cluster in the oxygen-evolving complex (OEC) of photosystem II (PS II) are: 1) What are the oxidation state(s) and structural changes in the Mn complex as the OEC proceeds through the S-state cycle? and (2) What is the mechanism by which four electrons are removed from two water molecules by the Mn complex to produce an O_2 molecule? We have addressed these questions principally by the use of X-ray absorption near edge structure (XANES), $K\beta$ X-ray emission spectroscopy (XES) and extended X-ray absorption fine structure (EXAFS) along with electron paramagnetic resonance spectroscopy (Robblee et al. 2001; Yachandra et al. 1996).

X-ray spectroscopy is element specific and can monitor Mn (or Ca/Sr) directly in the membrane; hence, it is a good method for studying the structure of the Mn-OEC without interference from pigment molecules, the lipid and protein matrix, or other metals such as Ca, Mg, Cu, or Fe which are present in active PS II preparations. Mn K-edge XANES and $K\beta$ XES provide information about oxidation states and the site symmetry of the Mn complex, and EXAFS at the Mn/Sr/Ca K-edge furnishes information about the number, type and distances to neighboring ligand atoms in the S_0, S_1, S_2 and S_3 states of the OEC (Yachandra 1995; Yachandra & Klein 1996). X-ray spectroscopy does not require long-range order; the structural studies can be performed on frozen solutions. Several of the intermediate states mentioned above can be stabilized as frozen solutions. Few other spectroscopic techniques provide such specificity for studying the structure of Mn in the OEC.

This presentation focuses on the application of X-ray spectroscopic methods to resolve structural questions regarding the Mn cluster in the OEC and we present our view of the structure

of the Mn cluster which is refined based on new data, and a mechanism for water oxidation that emphasizes the recent results from our laboratory.

2. Oxidation States of the Mn cluster

A key question for the understanding of photosynthetic water oxidation is whether the four oxidizing equivalents generated by the reaction center are accumulated on the four Mn ions of the OEC during S-state turnover, or whether a ligand-centered oxidation takes place, especially, before the formation and release of molecular oxygen during the S_3 to (S_4) to S_0 transition. We have addressed these questions by using Mn K-edge XANES (1s-4p absorption), $K\beta$ XES (3p-1s emission) and the recently introduced resonant inelastic X-ray scattering spectroscopy (RIXS) (1s to 3d/4p absorption followed by 2p-1s $K\alpha$ emission) to obtain L-edge-like spectra (2p-3d absorption).

A promising approach to study the Mn oxidation states in the native S-states is to step samples through the S-state cycle by the application of saturating single-turnover flashes and to characterize these samples by X-ray spectroscopy. We reported earlier XANES data from samples in the S_0 through S_3 states produced under these physiologically relevant conditions (Roelofs et al. 1996). The flash-advanced PS II samples prepared from spinach exhibited XANES spectra that showed Mn oxidation from S_0 to S_1 and from S_1 to S_2, but no further oxidation during the S_2 to S_3 transition. These results are consistent with our earlier studies by Guiles *et al*. that were prepared by illumination at low temperature, or by chemical treatment (Guiles et al. 1990a; Guiles et al. 1990b).

Other spectroscopic techniques like NMR-PRE (Sharp 1992), EPR (Ahrling et al. 1997; Dismukes & Siderer 1981; Hansson & Andréasson 1982; Messinger et al. 1997b), UV

absorption (Dekker 1992; Van Leeuwen et al. 1993) and Y_D^{ox} EPR/spin echo (Styring & Rutherford 1988) studies show that, in PS II, the S_0 to S_1 and S_1 to S_2 transitions are Mn-centered oxidations, and most groups agree that Mn redox states in the S_1 are (III_2, IV_2) which are oxidized to (III, IV_3) in the S_2 state. There is, however, a long standing controversy as to whether a Mn- or ligand-centered oxidation occurs in the S_2 to S_3 transition (Iuzzolino et al. 1998; Ono et al. 1992).

To resolve the controversy we used high-resolution Mn Kβ X-ray fluorescence (XES) studies in collaboration with Dr. Steve Cramer, who has constructed an unique high-resolution emission spectrometer that operates at the Mn Kβ fluorescence energy and has demonstrated the feasibility of determining the oxidation states of Mn (Bergmann & Cramer 1998). We have completed a comprehensive Mn Kβ XES study in conjunction with XANES on sets of samples prepared in a similar manner and characterized by EPR (Messinger et al. 2001).

Because the actual S-state composition is of critical importance to the interpretation of the results, we characterized the samples by EPR spectroscopy, using the S_2 multiline EPR signal (MLS) as a direct measure for the amount of S_2 in our samples (Fig. 1). The relative S-state populations in samples given 0, 1, 2, 3, 4, 5 or 6 flashes were determined from fitting the flash-induced EPR multiline signal oscillation pattern to the Kok model (Kok et al. 1970) for each of the samples used in the X-ray spectroscopy experiments. It is essential to obtain high concentrations of PS II in the S-states to obtain EPR, XANES and Kβ spectroscopy data with a good S/N ratio. A Nd-YAG laser system (Spectra-Physics PRO 230-10, 800 mJ/pulse at 532 nm, 9 ns pulse width) was used to illuminate PS II samples from both sides simultaneously. Because the pulse widths are narrow compared to those of a flash lamp, double hits become negligible. The damping of the oscillation pattern is minimized, thus making it possible to derive an unique

set of spectra by deconvolution. When the system becomes scrambled by frequent misses and double hits, the deconvolved spectra are not unique.

a) <u>Mn K-edge XANES</u> Our edge data are of sufficient S/N quality to allow for not only a determination of the absorption edge position (using the inflection point energy, defined as the zero-crossing in the second derivative of the edge), but also an analysis of the structure on the edge as a function of the number of flashes.

The edge spectra of samples given 0, 1, 2, or 3 flashes are combined with EPR information to calculate the pure S-state edge spectra. The shifts in inflection point energy positions and changes in shape are determined by second derivatives of the K-edge spectra and are shown in Fig. 2. In addition to the shift in edge position, the S_0 to S_1 (2.1 eV) and S_1 to S_2 (1.1 eV) transitions are accompanied by characteristic changes in the shape of the edge, also indicative of Mn-oxidation. The edge position shifts very little (0.3 eV) for the S_2 to S_3 transition, and the edge shape shows only minor changes (Messinger et al. 2001).

b) <u>Kβ X-ray Emission Spectroscopy (XES)</u> High-resolution Mn X-ray emission spectroscopy was performed on S_0, S_1, S_2 and S_3 samples prepared by using high-power laser flashes as described above. In this technique, the energy of the Mn Kβ emission (3p $\rightarrow$ 1s) is measured with a high-resolution dispersive spectrometer. The shape and energy of the $K\beta_{1,3}$ emission reflect the oxidation state(s) of the emitting Mn atom(s). The emission occurs from a 3p level that is mainly influenced by the number of unpaired 3d electrons and is less sensitive to the symmetry and bonding than the K-edge absorption, which involves transitions to the 4p level (Peng et al. 1994). The spin of the unpaired 3d valence electrons can be either parallel ($K\beta'$) or antiparallel ($K\beta_{1,3}$) to the hole in the 3p level. The splitting between the $K\beta'$ and $K\beta_{1,3}$ peaks becomes smaller for higher oxidation states because fewer 3d electrons interact with the 3p hole.

Thus, in contrast to the inflection points of the XANES edges, the $K\beta_{1,3}$ peaks shift to lower energy with higher oxidation states.

Using a 1st-moment analysis, the position of the main $K\beta_{1,3}$ peak has been calculated for each S-state. Based on the shifts, or lack thereof, of the 1st moments, we concluded that Mn is not oxidized during the $S_2 \rightarrow S_3$ transition. Our results (shown as difference spectra in Fig. 2) show a shift in energy between the S_0 and S_1 state spectra and between the S_1 and S_2 state spectra and seen in the derivative-shaped difference spectra. However, there is very little change between the S_2 and S_3 states, as seen in the difference spectrum (Messinger et al. 2001).

We have used two independent spectroscopic techniques, $K\beta$ and XANES spectroscopy, along with EPR, to examine the Mn redox states in PS II. Figure 3 summarizes the oscillation patterns of the 1st moments from the $K\beta_{1,3}$ spectra and of the XANES spectra inflection point energies. Both patterns show large shifts between the 0F and 1F samples, which reflect the Mn-centered oxidation during the $S_1 \rightarrow S_2$ transition. A much smaller shift occurs between 1F and 2F samples, which is inconsistent with a Mn-centered oxidation during the $S_2 \rightarrow S_3$ transition. The 2nd derivatives of the S-state XANES spectra and the $K\beta$ difference spectra (Fig. 2) confirm this conclusion. It is unlikely that both techniques would fail to detect a Mn-centered oxidation for the $S_2 \rightarrow S_3$ transition if it did, in fact, occur. Support for this conclusion has also come from XANES and $K\beta$ studies of two sets of structurally homologous Mn compounds in different oxidation states (Visser et al. 2001). We conclude that probably no direct Mn-oxidation is involved in this transition. The proposed Mn oxidation state assignments are as follows: S_0 (II, III, IV, IV) or (III, III, III, IV); S_1 (III, III, IV, IV); S_2 (III, IV, IV, IV); S_3 (III, IV, IV, IV) (Messinger et al. 2001).

c) <u>Resonant Inelastic X-ray Scattering Spectroscopy - RIXS</u> Mn L-edge spectra have several advantages over Mn K-edge spectra, because multiplet calculations can be applied to L-edge spectra which are sensitive to the number of holes in the 3d level, the oxidation state of Mn, and the spin state of Mn. This is a rich amount of information about oxidation states relative to what is available from K-edge XANES spectra. L-edge spectra have already been obtained for a number of Fe, Cu, and Ni metalloproteins, and have been simulated using multiplet calculations to provide quantitative conclusions about the oxidation states of the metals involved (Wang et al. 1997; Wang et al. 1996). However, the main disadvantage of using soft X-rays, where the Mn L-edge occurs (~650 eV), is that the samples are subjected to ultra high vacuum and are more prone to X-ray damage.

We have recently started exploring the technique of resonant inelastic scattering (RIXS) that circumvents the problems mentioned above in a very elegant manner. It is possible to combine the two types of K- and L-edge experiments by mapping the 1s2p resonant inelastic scattering (RIXS) landscape as shown in Fig. 4 in a simplified two-step process (Caliebe et al. 1998). RIXS involves exciting a pre-edge transition (1s to 3d) of the K shell using hard X-rays. Then, the high-resolution X-ray emission analyzer can be tuned to detect the Kα fluorescence of Mn, which is a 2p to 1s transition. The final state from this transition is a 2p hole, which is the same final state as the L-edge fluorescence (3d to 2p). An advantage of RIXS over both conventional techniques is that the resonances are separated according to the final states they decay into. As a result, the resonances appear as islands in the resonant landscape and their spectral shapes can be analyzed. A two-dimensional RIXS spectrum is obtained by plotting the scanned incident X-ray energy, ν (1s to 3d), versus E_B, the binding energy, which is equal to (ν - f), f is the energy of the scanned high resolution X-ray emission analyzer. Furthermore, this

8

technique offers an unprecedented opportunity to selectively excite into specific molecular orbitals with 3d character by tuning the incoming X-rays to look at a specific pre-edge transition; at least 2 – 3 resolvable pre-edge transitions are seen in the Mn K-edge spectrum of PS II. This means that it would be possible to obtain 'nested' RIXS spectra which correspond to fluorescence from different molecular orbitals with 3d character.

We have collected preliminary data from a PS II sample in the S_1 and S_2 states. The shape and ratio of the L_{III}/L_{II}-like peaks of the PS II RIXS spectrum are in between those for the Mn(III) and Mn(IV) complex, and very different from that for the Mn(II) complex. This indicates a mixed (III) and (IV) Mn oxidation state in the S_1 state - (III_2, IV_2); a conclusion in accord with that derived from other studies. The cross sections of the 2D-RIXS spectra reveal the L-edge-like character, showing two well-resolved peaks due to spin-orbit coupled states J=3/2 (L_{III}-like edge) and J=1/2 (L_{II}-like edge). The ratio of the L_{III}/L_{II} peaks increases from (II) to (III) to (IV); the ratio for PS II changes from S_1 to S_2 in a manner consistent with an oxidation from $(III)_2(IV)_2$ to $(III)(IV)_3$.

3. Structure of the Manganese Cluster

We have used Mn EXAFS to study the local structure of the Mn complex and have proposed topologically consistent models that can be reconciled with several structural arrangements of the four Mn atoms (DeRose et al. 1994). The proposed model consists of two or three di-μ-oxo bridged binuclear Mn units with Mn-Mn distances of ~2.7 Å that are linked to each other by a mono-μ-oxo bridge with a Mn-Mn separation of ~3.3 Å, and with Ca at a distance of 3.4 Å to Mn (DeRose et al. 1994; Yachandra et al. 1993). The Mn-Mn distances are largely invariant in the native S_1 and S_2 states (DeRose et al. 1994). EXAFS experiments on the

S_3 and S_0 states have been difficult to perform on PS II samples using single flashes. The requirement of optically dilute samples to ensure saturation by single actinic flashes generally results in a low signal-to-noise ratio. We have recently been able to extend these studies to the S_3 and S_0 states prepared by flash illumination.

a) S_3 State Earlier EXAFS data from the chemically treated S_3 state samples produced by a double turnover method indicated that the two di-μ-oxo-bridged Mn-Mn dimer units may become nonequivalent (Guiles et al. 1990b). The EXAFS spectra from calcium-depleted S_3' samples ($S_2Y_Z^{\bullet}$) prepared by low pH treatment in a citrate buffer do not exhibit similar heterogeneity in 2.7 Å Mn-Mn distances (Latimer et al. 1998).

EXAFS data of S_3 samples created under physiological conditions with saturating flash illumination show significant changes in the Mn-Mn distances in the S_3 state compared to the S_1 and the S_2 states. The two 2.7 Å Mn-Mn distances that characterize the di-μ-oxo centers in the S_1 and S_2 states are lengthened to ~2.8 and 3.0 Å in the S_3 state, respectively (Fig. 5). The 3.3 Å Mn-Mn and Mn-Ca distances also increase by 0.04-0.2 Å. These changes in Mn-Mn distances are interpreted as consequences of the onset of substrate water oxidation in the S_3 state. Mn-centered oxidation is evident during the S_0 to S_1 and S_1 to S_2 transitions. During the S_2 to S_3 transition, we propose that the changes in Mn-Mn distances are the result of ligand or water oxidation, leading to the formation of an oxyl radical intermediate formed at a bridging or terminal position. We propose that substrate/water oxidation occurring at this transition provides the trigger for the formation of the O-O bond; the critical step in the water oxidation reaction. The reaction of the oxyl radical with OH^-, H_2O, or an oxo group during the subsequent S-state conversion is proposed to lead to the formation of the O-O bond (Liang et al. 2000).

b) S_0 State   Although many topological structures have been proposed, on the basis of EXAFS (Dau et al. 2001; Penner-Hahn 1998; Robblee et al. 2001) and EPR (Hasegawa et al. 1999a; Peloquin & Britt 2001) studies for the Mn cluster in PS II, the issue of whether there are two, or three di-μ-oxo bridged moieties in the Mn cluster has been an open question. However, a determination of the exact number of such interactions is important for narrowing the number of options from the many that have been proposed. We have obtained data from the S_0 state that shows that there may be three di-μ-oxo bridged motifs that are characterized by the ~2.7 Å Mn-Mn distance.

The S_0 samples were generated by three flash illumination followed by incubation with FCCP (Messinger et al. 1997a). The multiline EPR spectra of the S_0 and S_2 states were used to characterize all the samples.

Figure 6 shows the Fourier transforms of the k^3-weighted EXAFS data from the S_0 and S_1 states. The Fourier peak II was isolated and fit to the EXAFS equation with one or two distances for the S_0 and S_1 states. Since there has to be an integral number of Mn-Mn interactions, the fits were constrained to a ratio of 1:1 and 2:1 for the two Mn-Mn interactions. The fits for the S_1 state showed that the two distances are separated by significantly less than what can be resolved using the data set at present. However, the situation is very different for the fits for the S_0 state. The quality of fit parameter, ε^2 value, improved considerably on going from a one-shell to a two-shell fit, especially, for the case of the 2:1 ratio of Mn-Mn interactions. The result of the fitting provides evidence that there may be three short (~2.7 to 2.8 Å) Mn-Mn interactions in the Mn cluster.

Figure 7 shows the best fits to two Mn-Mn distances for the S_0 state as a function of the number of each of the Mn-Mn interactions. The contour plot graphically illustrates that the

11

global minimum at two Mn-Mn interactions at 2.7 Å and one Mn-Mn interaction at 2.85 Å is very well defined, and hence gives us confidence in its reliability. We have re-examined the data from the S_0*, the g=4.1 S_2, the NH_3- or F$^-$-inhibited S_2, and the S_3 states, where we have shown that there is distance heterogeneity in the Mn-Mn vectors. In each case, the ratio of the number of the two Mn-Mn interactions was ~2:1. This leads us to think that there may be three Mn interactions at ~2.7 Å in the Mn cluster in its native state, one of which is perturbed in the S_0, F$^-$- and NH_3-inhibited S_2 and the g=4.1 S_2 states, and all three are perturbed in the S_3 state.

We showed earlier that there are several topological models that are compatible with our EXAFS data. These models have been described in detail (DeRose et al. 1994; Robblee et al. 2001). However, only one of those options (A) is widely used as a working model, although options E, F and G (the nomenclature is from DeRose *et al*. 1994) have been shown to be preferred on the basis of EPR and ENDOR simulations [Peloquin, 2001 #2099; (Hasegawa et al. 1999b). On the basis of the present results from the S_0 state, we think it is important to consider the options that include three di-μ-oxo bridged moieties in the Mn cluster. Figure 8 shows several such options, G, I, and J, that were proposed earlier, and two newer options, L and M, among several others that can be conceived. Options J and I are less likely structures because J lacks a Mn-Mn interaction at 3.3 Å, and I has two such interactions. The EXAFS data from an inorganic compound (Auger et al. 1990) with the motif in option J is very different from that obtained from a PS II sample (unpublished data). Options G, L and M all have three di-μ-oxo bridges and one mono-μ-oxo bridge; that is three 2.7 Å and one 3.3 Å Mn-Mn interaction and are qualitatively in agreement with the asymmetry seen in the electron density of the Mn cluster (Zouni et al. 2001). Options L and M are also similar to the structure proposed on the basis of density functional theory calculations (Siegbahn 2000). We are in the process of testing the

compatibility of various Mn models that satisfy the criteria set by the distance data and orientation of the various Mn-Mn/Ca vectors obtained from EXAFS with the electron density data obtained from X-ray crystallography.

3. The Role of the Ca Cofactor

Calcium and chloride are necessary cofactors for the proper function of the OEC of PS II (Debus 1992). While the Mn complex has been extensively studied by X-ray absorption techniques (XANES and EXAFS) comparatively less is known about the Ca^{2+} cofactor. The fewer number of studies on the Ca^{2+} cofactor have sometimes relied on substituting the native cofactor with strontium or other metals (Boussac & Rutherford 1988; Ghanotakis et al. 1985) and have stirred some debate about the structure of the binding site. Past efforts using Mn EXAFS on Sr-substituted PS II are suggestive of a close link between the Mn cluster and Sr, within 3.5 Å (Latimer et al. 1995). The most recent published study using Sr EXAFS on similar samples confirms this finding of a 3.5 Å distance between Mn and Sr (Cinco et al. 1998). This finding was based on a second Fourier peak in the Sr EXAFS from functional samples, but is absent from inactive, hydroxylamine-treated PS II. This Fourier peak II was found to fit best to two Mn at 3.5 Å rather than lighter atoms (carbon). Nevertheless, other experiments have given contrary results (RiggsGelasco et al. 1996).

a) <u>Oriented Sr EXAFS</u> We have extended the technique by using polarized Sr EXAFS on layered Sr-substituted samples, to provide important angle information. Polarized EXAFS involves collecting spectra for different incident angles (θ) between the membrane normal of the layered sample and the X-ray electric field vector. Dichroism in the EXAFS can occur, depending on how the particular absorber–backscatterer (A–B) vector is aligned with the electric

field. Through analysis of the dichroism, we extract the average orientation (ϕ) of this A–B

vector relative to the membrane normal, and the average number of scatterers per absorbing atom

(N_{iso}). Constraints on the structural model are then imposed by these parameters.

Sr-substituted PS II samples were made by a process of Ca depletion, Sr^{2+} reactivation,

and Chelex treatment to remove excess Sr (Cinco et al. 1998). Oriented samples were made by

layering onto flat Mylar films (Dau et al. 1995; Mukerji et al. 1994). The Fourier transforms

from the polarized Sr EXAFS showed extreme dichroism in Fourier peak II (Figure 9).

Nonlinear least-squares regression analysis produced the solid curve shown in Figure 9 as the

best fit of the 15 data points (angles from six separate samples) and the result translates to 1–2

Sr–Mn vectors with an average angle of 23 ± 4° from the membrane normal.

The orientation data from the Sr EXAFS experiments can be combined with the

dichroism data from Mn EXAFS data to calculate the orientation of the 3.3 Å Mn–Mn vector.

Fourier Peak III in the Mn EXAFS which contains Mn–Mn (3.3 Å) and Mn–Ca (3.4 Å)

contributions, is dichroic, with an average angle of 43 ± 10° with respect to the membrane

normal (Mukerji et al. 1994). By including the Mn-Ca vector at 23°, we calculate an angle of ~

62° for the 3.3 Å Mn–Mn vector. Previous polarized Mn EXAFS experiments on PS II have

shown angles of 55° and 67° for the 2.7 Å Mn–Mn vectors (Dau et al. 1995; Mukerji et al. 1994).

All Mn–Mn vectors then lie at roughly the same angle (~60°) with respect to the membrane

plane, but are not restricted to being collinear, because the PS II membranes are ordered in one

dimension only.

b) Ca EXAFS In a complementary and definitive experiment, we have used Ca K-edge

EXAFS studies to probe the binding site of the native cofactor for any nearby Mn, within ~ 4 Å.

This is analogous to the Sr EXAFS studies already published (Cinco et al. 1998), but it focuses

on the native cofactor and avoids the treatments involving Ca depletion and Sr substitution. This technique is a more sensitive and direct probe of the Ca binding site in PS II than Sr EXAFS.

Chelex-treated PS II (2Ca/4Mn/PS II) was accumulated on the flat surface of solid Plexiglas (Ca-free) while not affecting oxygen-evolving activity or the S_2 EPR multiline signal. To prepare the parallel control (inactive) sample, 40 μL of hydroxylamine (NH_2OH, 100 mM) was added to the surface of the layered PS II, was allowed to soak and dry without loss of PS II material.

The Fourier transform of the Ca EXAFS is presented in Figure 10. The spectra are remarkably similar to the Fourier transforms of the earlier Sr EXAFS study with Sr substituted for Ca. The first (largest) Fourier peak corresponds to the coordinating oxygen atoms closest to calcium. In contrast to the control (NH_2OH-treated) sample, the Chelex-treated PS II shows a second Fourier peak. When this peak II is isolated and simulated with possible scattering atoms, it corresponded best to Mn at 3.4 Å, rather than to light atom (C, O or Cl) neighbors. These results were consistent with the earlier Sr EXAFS studies (Cinco et al. 1998).

The Ca EXAFS protocol has directly probed the Ca cofactor in its native state, avoiding potentially disruptive treatments such as the low pH exposure involved in metal substitution. This result provides proof of the Mn/Ca heteronuclear cluster as the catalytic site of oxygen evolution in PS II.

Because significant angle information about Mn–Mn and Mn–Ca vectors is now available as described above, other topological models previously discussed (DeRose et al. 1994) can be refined to include the presence of Ca and account for the dichroism data. Three possible refined models are presented in Figure 11. Recent EXAFS data from the S_0 state has indicated

15

that there maybe three di-μ-oxo bridged Mn-Mn units (see above). However, such motifs were not included in Figure 11, but considering them is a subject for future work.

4. Mechanism of Water Oxidation

The many mechanisms of water oxidation that have been proposed can be broadly divided into four groups, in which the kind of oxygen atom (Mn-terminal oxygen ligand , Mn-bridging oxygen ligand or exogenous oxygen from water or hydroxide) involved in O-O bond formation is different. In these four groups the oxygen atoms can de derived from two terminal oxygens bound to Mn atoms (Haumann & Junge 1999; Hillier & Wydrzynski 2001; Hoganson & Babcock 2000; Limburg et al. 2000; Messinger et al. 2001; Renger 2001; Robblee et al. 2001), one bridging or terminal oxygen and one exogenous oxygen (Dau et al. 2001; Hillier & Wydrzynski 2001; Kuzek & Pace 2001; Messinger et al. 2001; Robblee et al. 2001; Siegbahn & Crabtree 1999; Vrettos et al. 2001), one terminal and one bridging oxygen (Limburg et al. 2000; Nugent et al. 2001), or two bridging oxygens (Brudvig & Crabtree 1986; Christou & Vincent 1987; Messinger et al. 2001; Robblee et al. 2001). The results that have a direct bearing on this subject are the $H_2^{16}O/H_2^{18}O$ exchange studies by Messinger and coworkers that support the presence of two non-equivalent exchangeable sites in the S_3 state (Hillier et al. 1998; Messinger et al. 1995).

We have proposed earlier a model for the S_3 state in which an oxyl radical is generated on one of the μ-oxo-bridges, which results in an increase of one of the Mn–Mn distances to ~2.95 Å (Figure 5) (Liang et al. 2000; Yachandra et al. 1996). Consistent with our XANES results is the implication in this structure that the oxidative equivalent is not stored on the Mn atoms *per se* during the $S_2 \rightarrow S_3$ transition but is delocalized with significant charge and spin density on the

bridging oxo ligand. These data are reinforced by our Mn Kβ emission studies of the various S-states (Messinger et al. 2001). Second, the Mn–Mn distance in both of the di-μ-oxo-bridged units increases from 2.72 Å to 2.82 Å and 2.95 Å, upon the formation of the S_3 state. These changes imply a significant structural change in the Mn cluster as it proceeds to the S_3 state. It is difficult to rationalize such changes in Mn–Mn distance as arising purely from Mn oxidation, or involving Mn terminal ligands. It is difficult to understand how changes in terminal ligation can generate such a profound change on the Mn–Mn distances in the S_3 state. Replacement of terminal ligands in di-μ-oxo bridged model compounds has a minimal effect on the Mn–Mn distance of 2.7 Å that is characteristic of such di-μ-oxo bridged Mn compounds (Pecoraro 1992; Wieghardt 1989). However, it is easier to rationalize increases in Mn–Mn distances as being due to changes in the bridging structure. We propose that substrate/water oxidation chemistry is occurring at the S_2 to S_3 transition as evidenced by the lack of Mn oxidation, and leading to the significant structural changes as seen in the increase in the Mn-Mn distances. Our proposed mechanism, where the O-O bond is formed between one critical bridging oxygen and another oxygen atom derived from a bridging/terminal oxygen ligand or an exogenous oxygen also avoids the formation of the O–O bond until the most oxidized state (S_4) is reached. This precludes the formation and release of peroxide or other oxidation products of water in the earlier S-states, thus preventing the system from 'short circuiting' and avoiding the risk of damaging the polypeptides of PS II.

Acknowledgements

References

Ahrling, K. A., Peterson, S. & Styring, S. 1997 An oscillating manganese electron paramagnetic resonance signal from the S_0 state of the oxygen evolving complex in photosystem II. *Biochemistry* **36**, 13148-13152.

Auger, N., Girerd, J.-J., Corbella, M., Gleizes, A. & Zimmermann, J.-L. 1990 Synthesis, structure, and magnetic properties of the stable triangular [Mn(IV)3O4]4+ core. *J. Am. Chem. Soc.* **112**, 448-50.

Bergmann, U. & Cramer, S. P. 1998 A high-resolution large-acceptance analyzer for x-ray fluorescence and Raman spectroscopy. In *SPIE Conference on Crystal and Multilayer Optics*, vol. 3448, pp. 198-210. San Diego, CA: SPIE.

Boussac, A. & Rutherford, A. W. 1988 Nature of the Inhibition of the Oxygen-Evolving Enzyme of Photosystem-II Induced By Nacl Washing and Reversed By the Addition of Ca^{2+} or Sr^{2+}. *Biochemistry* **27**, 3476-3483.

Brudvig, G. W. & Crabtree, R. H. 1986 Mechanism for photosynthetic oxygen evolution. *Proc. Natl. Acad. Sci. U. S. A.* **83**, 4586-8.

Caliebe, W. A., Kao, C.-C., Hastings, J. B., Taguchi, M., Kotani, A., Uozumi, T. & DeGroot, F. M. F. 1998 1s2p resonant inelastic x-ray scattering in α-FeO_3. *Physical Review B* **58**, 13542-13458.

Christou, G. & Vincent, J. B. 1987 The Molecular Double-Pivot Mechanism For Water Oxidation. *Biochim. Biophys. Acta* **895**, 259-274.

Cinco, R. M., Robblee, J. H., Rompel, A., Fernandez, C., Yachandra, V. K., Sauer, K. & Klein, M. P. 1998 Strontium EXAFS reveals the proximity of calcium to the manganese cluster of oxygen-evolving photosystem II. *Journal of Physical Chemistry B* **102**, 8248-8256.

Dau, H., Andrews, J. C., Roelofs, T. A., Latimer, M. J., Liang, W. C., Yachandra, V. K., Sauer, K. & Klein, M. P. 1995 Structural Consequences of Ammonia Binding to the Manganese Center of the Photosynthetic Oxygen-Evolving Complex - an X- Ray-Absorption Spectroscopy Study of Isotropic and Oriented Photosystem-Ii Particles. *Biochemistry* **34**, 5274-5287.

Dau, H., Iuzzolino, L. & Dittmer, J. 2001 The tetra-manganese complex of photosystem II during its redox cycle - X-ray absorption results and mechanistic implications. *Biochim. Biophys. Acta* **1503**, 24-39.

Debus, R. J. 1992 The Manganese and Calcium-Ions of Photosynthetic Oxygen Evolution. *Biochim. Biophys. Acta* **1102**, 269-352.

Dekker, J. P. 1992 Optical studies on the oxygen-evolving complex of photosystem II. In *Manganese Redox Enzymes* (ed. V. L. Pecoraro), pp. 85-103. New York: VCH Publishers.

DeRose, V. J., Mukerji, I., Latimer, M. J., Yachandra, V. K., Sauer, K. & Klein, M. P. 1994 Comparison of the Manganese Oxygen-Evolving Complex in Photosystem II of Spinach and Synechococcus Sp With Multinuclear Manganese Model Compounds By X-Ray Absorption Spectroscopy. *J. Am. Chem. Soc.* **116**, 5239-5249.

Dismukes, G. C. & Siderer, Y. 1981 Intermediates of a Polynuclear Manganese Center Involved in Photosynthetic Oxidation of Water. *Proc. Nat'l Acad. Sci. USA* **78**, 274-278.

Ghanotakis, D. F., Babcock, G. T. & Yocum, C. F. 1985 Structure of the oxygen-evolving complex of photosystem II: calcium and lanthanum compete for sites on the oxidizing side of photosystem II which control the binding of water-soluble polypeptides and regulate the activity of the manganese complex. *Biochim. Biophys. Acta* **809**, 173-80.

Guiles, R. D., Yachandra, V. K., McDermott, A. E., Cole, J. L., Dexheimer, S. L., Britt, R. D., Sauer, K. & Klein, M. P. 1990a The S_0 State of Photosystem-Ii Induced By Hydroxylamine - Differences Between the Structure of the Manganese Complex in the S_0 and S_1 States Determined By X-Ray Absorption- Spectroscopy. *Biochemistry* **29**, 486-496.

Guiles, R. D., Zimmermann, J.-L., McDermott, A. E., Yachandra, V. K., Cole, J. L., Dexheimer, S. L., Britt, R. D., Wieghardt, K., Bossek, U., Sauer, K. & Klein, M. P. 1990b The S_3 state of photosystem II: differences between the structure of the manganese complex in the S_2 and S_3 states determined by x-ray absorption spectroscopy. *Biochemistry* **29**, 471-85.

Hansson, Ö. & Andréasson, L.-E. 1982 EPR-detectable magnetically interacting manganese ions in the photosynthetic oxygen-evolving system after continuous illumination. *Biochim. Biophys. Acta* **679**, 261-8.

Hasegawa, K., Ono, T.-a., Inoue, Y. & Kusunoki, M. 1999a How to evaluate the structure of a tetranuclear Mn cluster from magnetic and EXAFS data: case of the S_2-state Mn-cluster in photosystem II. *Bull. Chem. Soc. Jpn.* **72**, 1013-1023.

Hasegawa, K., Ono, T.-a., Inoue, Y. & Kusunoki, M. 1999b Spin-exchange interactions in the S_2-state manganese tetramer in photosynthetic oxygen-evolving complex deduced from g=2 multiline EPR signal. *Chem. Phys. Lett.* **300**, 9-19.

Haumann, M. & Junge, W. 1999 Photosynthetic water oxidation: a simplex-scheme of its partial reactions. *Biochim. Biophys. Acta* **1411**, 86-91.

Hillier, W., Messinger, J. & Wydrzynski, T. 1998 Kinetic determination of the fast exchanging substrate water molecule in the S_3 state of photosystem II. *Biochemistry* **37**, 16908-16914.

Hillier, W. & Wydrzynski, T. 2001 Oxygen ligand exchange at metal sites - implications for the O_2 evolving mechanism of photosystem II. *Biochim. Biophys. Acta* **1503**, 197-209.

Hoganson, C. W. & Babcock, G. T. 2000 Mechanistic aspects of the tyrosyl radical-manganese complex in photosynthetic water oxidation. In *Manganese and Its Role in Biological Processes*, vol. 37 (ed. A. Sigel & H. Sigel), pp. 613-656. New York: Marcel Dekker Inc.

Iuzzolino, L., Dittmer, J., Dörner, W., Meyer-Klaucke, W. & Dau, H. 1998 X-ray absorption spectroscopy on layered photosystem II membrane particles suggests manganese-centered oxidation of the oxygen-evolving complex for the S_0-S_1, S_1-S_2, and S_2-S_3 transitions of the water oxidation cycle. *Biochemistry* **37**, 17112-17119.

Kok, B., Forbush, B. & McGloin, M. 1970 Cooperation of charges in photosynthetic oxygen evolution. I. A linear four step mechanism. *Photochem. Photobiol.* **11**, 457-475.

Kuzek, D. & Pace, R. J. 2001 Probing the Mn oxidation states in the OEC. Insights from spectroscopic, computational and kinetic data. *Biochim. Biophys. Acta* **1503**, 123-137.

Latimer, M. J., DeRose, V. J., Mukerji, I., Yachandra, V. K., Sauer, K. & Klein, M. P. 1995 Evidence For the Proximity of Calcium to the Manganese Cluster of Photosystem II - Determination By X-Ray-Absorption Spectroscopy. *Biochemistry* **34**, 10898-10909.

Latimer, M. J., DeRose, V. J., Yachandra, V. K., Sauer, K. & Klein, M. P. 1998 Structural effects of calcium depletion on the manganese cluster of photosystem II: Determination by X-ray absorption spectroscopy. *Journal of Physical Chemistry B* **102**, 8257-8265.

Liang, W., Roelofs, T. A., Cinco, R. M., Rompel, A., Latimer, M. J., Yu, W. O., Sauer, K., Klein, M. P. & Yachandra, V. K. 2000 Structural change of the Mn cluster during the S2->S3 state transition of the Oxygen-Evolving Complex of Photosystem II. Does it reflect the onset of water/substrate oxidation? Determination by Mn X-ray absorption spectroscopy. *J. Am. Chem. Soc.* **122**, 3399-3412.

Limburg, J., Brudvig, G. W. & Crabtree, R. H. 2000 Modeling the Oxygen-Evolving Complex in Photosystem II. In *Biomimetic oxidations catalyzed by transition metal complexes* (ed. B. Meunier), pp. 509-541. London: Imperial College Press.

Messinger, J., Badger, M. & Wydrzynski, T. 1995 Detection of One Slowly Exchanging Substrate Water Molecule in the S_3 State of Photosystem-Ii. *Proc. Natl. Acad. Sci. U. S. A.* **92**, 3209-3213.

Messinger, J., Nugent, J. H. A. & Evans, M. C. W. 1997a Detection of an EPR multiline signal for the S-0 state in photosystem II. *Biochemistry* **36**, 11055-11060.

Messinger, J., Robblee, J. H., Bergmann, U., Fernandez, C., Glatzel, P., Visser, H., Cinco, R. M., McFarlane, K. L., Bellacchio, E., Pizarro, S. A., Cramer, S. P., Sauer, K., Klein, M. P. & Yachandra, V. K. 2001 Absence of Mn-Centered Oxidation in the S_2 to S_3 Transition: Implications for the Mechanism of Photosynthetic Water Oxidation. *J. Am. Chem. Soc.* **123**, 7804-7820.

Messinger, J., Robblee, J. H., Yu, W. O., Sauer, K., Yachandra, V. K. & Klein, M. P. 1997b The S0 state of the oxygen-evolving complex in Photosystem II is paramagnetic: Detection of an EPR multiline signal. *J. Am. Chem. Soc.* **119**, 11349-11350.

Mukerji, I., Andrews, J. C., Derose, V. J., Latimer, M. J., Yachandra, V. K., Sauer, K. & Klein, M. P. 1994 Orientation of the Oxygen-Evolving Manganese Complex in a Photosystem-II Membrane Preparation - an X-Ray-Absorption Spectroscopy Study. *Biochemistry* **33**, 9712-9721.

Nugent, J. H. A., Rich, A. M. & Evans, M. C. W. 2001 Photosynthetic water oxidation: towards a mechanism. *Biochim. Biophys. Acta* **1503**, 138-146.

Ono, T., Noguchi, T., Inoue, Y., Kusunoki, M., Matsushita, T. & Oyanagi, H. 1992 X-Ray-Detection of the Period-4 Cycling of the Manganese Cluster in Photosynthetic Water Oxidizing Enzyme. *Science* **258**, 1335-1337.

Pecoraro, V. L. (ed) 1992 *Manganese Redox Enzymes* New York: VCH Publishers.

Peloquin, J. M. & Britt, R. D. 2001 EPR/ENDOR characterization of the Physical and Electronic Structure of the OEC Mn Cluster. *Biochim. Biophys. Acta* **1503**, 96-111.

Peng, G., DeGroot, F. M. F., Hämäläinen, K., Moore, J. A., Wang, X., Grush, M. M., Hastings, J. B., Siddons, D. P., Armstrong, W. H., Mullins, O. C. & Cramer, S. P. 1994 High-Resolution Manganese X-Ray-Fluorescence Spectroscopy - Oxidation-State and Spin-State Sensitivity. *J. Am. Chem. Soc.* **116**, 2914-2920.

Penner-Hahn, J. E. 1998 Structural characterization of the Mn site in the photosynthetic oxygen-evolving complex. *Struct. Bonding (Berlin)* **90**, 1-36.

Renger, G. 2001 Photosynthetic water oxidation to molecular oxygen: apparatus and mechanism. *Biochim. Biophys. Acta* **1503**, 210-228.

RiggsGelasco, P. J., Mei, R., Ghanotakis, D. F., Yocum, C. F. & PennerHahn, J. E. 1996 X-ray absorption spectroscopy of calcium-substituted derivatives of the oxygen-evolving complex of photosystem II. *J. Am. Chem. Soc.* **118**, 2400-2410.

Robblee, J. H., Cinco, R. M. & Yachandra, V. K. 2001 X-ray spectroscopy-based structure of the Mn cluster and mechanism of photosynthetic oxygen evolution. *Biochim. Biophys. Acta* **1503**, 7-23.

Roelofs, T. A., Liang, M. C., Latimer, M. J., Cinco, R. M., Rompel, A., Andrews, J. C., Sauer, K., Yachandra, V. K. & Klein, M. P. 1996 Oxidation states of the manganese cluster during

the flash-induced S-state cycle of the photosynthetic oxygen-evolving complex. *Proc. Natl. Acad. Sci. U.S.A.* **93**, 3335-3340.

Sharp, R. R. 1992 Proton NMR relaxation due to the photosynthetic oxygen-evolving center. In *Manganese Redox Enzymes* (ed. V. L. Pecoraro), pp. 177-96. New York: VCH Publishers.

Siegbahn, P. E. M. 2000 Theoretical Models for the Oxygen Radical Mechanism of Water Oxidation and of the Water Oxidizing Complex of Photosystem II. *Inorg. Chem.* **39**, 2923-2935.

Siegbahn, P. E. M. & Crabtree, R. H. 1999 Manganese oxyl radical intermediates and O-O bond formation in photosynthetic oxygen evolution and a proposed role for the calcium cofactor in photosystem II. *J. Am. Chem. Soc.* **121**, 117-127.

Styring, S. A. & Rutherford, A. W. 1988 The Microwave-Power Saturation of SII_{slow} Varies With the Redox State of the Oxygen-Evolving Complex in Photosystem-II. *Biochemistry* **27**, 4915-4923.

Vanleeuwen, P. J., Heimann, C. & Vangorkom, H. J. 1993 Absorbency Difference Spectra of the S-State Transitions in Photosystem-Ii Core Particles. *Photosynthesis Research* **38**, 323-330.

Visser, H., Anxolabéhère-Mallart, E., Bergman, U., Glatzel, P., Robblee, J. H., Cramer, S. P., Girerd, J.-J., Sauer, K., Klein, M. P. & Yachandra, V. K. 2001 Mn K-edge XANES and Kβ XES Studies of Two Mn-oxo Binuclear Complexes. Investigation of Three Different Oxidation States Relevant to the Oxygen-Evolving Complex of PhotosystemII. *J. Am. Chem. Soc.* **123**, 7031-7039.

Vrettos, J. S., Limburg, J. & Brudvig, G. W. 2001 Mechanism of photosynthetic water oxidation: combining biophysical studies of photosystem II with inorganic model chemistry. *Biochim. Biophys. Acta* **1503**, 229-245.

Wang, H., Peng, G., Miller, L. M., Scheuring, E. M., George, S. J., Chance, M. R. & Cramer, S. P. 1997 Iron L-Edge X-ray Absorption Spectroscopy of Myoglobin Complexes and Photolysis Products. *J. Am. Chem. Soc.* **119**, 4921-4928.

Wang, X., de Groot, F. & Cramer, S. P. 1996 X-ray magnetic circular dichroism spectra and distortions at Fe^{2+} $L_{2,3}$ edges. *J. Electron Spectrosc. Relat. Phenom.* **78**, 337-40.

Wieghardt, K. 1989 The Active-Sites in Manganese-Containing Metalloproteins and Inorganic Model Complexes. *Angew. Chem. International Ed. in English* **28**, 1153-1172.

Yachandra, V. K. 1995 X-ray Absorption Spectroscopy and Applications in Structural Biology. In *Methods Enzymol.*, vol. 246 (ed. K. Sauer), pp. 638-675: Academic Press, Inc.

Yachandra, V. K., Derose, V. J., Latimer, M. J., Mukerji, I., Sauer, K. & Klein, M. P. 1993 Where Plants Make Oxygen - a Structural Model For the Photosynthetic Oxygen-Evolving Manganese Cluster. *Science* **260**, 675-679.

Yachandra, V. K. & Klein, M. P. 1996 X-ray absorption spectroscopy: determination of transition metal site structures in photosynthesis. *Adv. Photosynth.* **3**, 337-354.

Yachandra, V. K., Sauer, K. & Klein, M. P. 1996 Manganese cluster in photosynthesis: Where plants oxidize water to dioxygen. *Chem. Rev.* **96**, 2927-2950.

Zouni, A., Witt, H. T., Kern, J., Fromme, P., Krauss, N., Saenger, W. & Orth, P. 2001 Crystal structure of photosystem II from Synechococcus elongatus at 3.8 angstrom resolution. *Nature* **409**, 739-743.

Figure Captions

Figure 1. The S_2 multiline EPR signal amplitudes are shown as a function of flash number (solid line). The best fit to the S_2 multiline oscillation pattern is shown as a dashed line. The S-state compositions of the samples are derived from the fit. Individual S-State spectra can be uniquely determined from these data, if the oscillation pattern is as pronounced as shown in the Figure. It is important that a deep oscillation pattern is obtained, because all subsequent steps that are used in the deconvolution to generate pure S-state spectra are critically dependent on this data.

Figure 2. A): Second derivatives of the normalized pure S-state Mn K-edge spectra of the Mn-cluster of PS II. For clarity a vertical dashed line has been drawn at the inflection-point energy (IPE) of the S_1-state. The change in IPE (Δ in eV) for each S-state advance is given at the right. For reference, the K-edge spectrum of the S_1-state is plotted as well (dashed line). B): The S_1-S_0, S_2-S_1, S_3-S_2, and S_0-S_3 difference high resolution Mn X-ray Kβ-emission spectra. The derivative shapes indicate shifts in the energy of the spectra between the S_0 and S_1, and S_1 and S_2 spectra, indicating oxidations of Mn. The S_3-S_2 difference spectra demonstrates the similarity of the spectra, suggesting that this advance does not involve a Mn centered oxidation.

Figure 3. A) Inflection-point energy (IPE, in eV) of the Mn K-edge of PS II membranes as a function of the number of applied flashes. B) The first moments of the Mn Kβ fluorescence spectra (<E>) as a function of flash number. The Mn K-edge shifts to higher energy as Mn is oxidized. The first moment of the Mn Kβ fluorescence shifts to lower energy as Mn is oxidized.

The complementary and mutually reinforcing results provide a strong case for Mn oxidation during the S_0 to S_1 and S_1 and S_2 advances but no Mn-centered oxidation at the S_2 to S_3 advance.

Figure 4. The electronic energy diagram of the transitions that occur in Mn K-edge, L-edge and RIXS spectroscopy. L-edge like information is extracted from RIXS by subtracting the emission energy, f, from the excitation energy, υ (energy transfer, $(\upsilon - f)$ vs the incident energy, υ). However, more final states are present in the RIXS spectra than in the L-edge spectra. Therefore, RIXS gives a wealth of information about the Mn oxidation state, ligand environment and local symmetry.

Figure 5. A): Fourier-filtered k-space EXAFS data from S_2 (dashed line) and S_3 (solid line) state of PS II samples. The differences in phase, frequency and amplitudes between the raw S_2 and S_3 state EXAFS spectra are very obvious in these spectra. B): Fourier transform power spectra of S_2 (dashed line) and S_3 (solid line) states of PS II. The major Fourier peaks are labeled I, II and III. The spectra are clearly different between the S_2 (dashed line) and S_3 states (solid line). There is a reduction in amplitude in all three peaks in the S_3 state compared to the S_2 state. More importantly, peaks II and III are at a greater apparent distance R' for the S_3 state compared to the S_2 state as shown.

Figure 6. Fourier Transforms of the S_0 (dashed line) and S_1 state (solid line) of the k^3-weighted Mn-EXAFS spectra (3.5 to 11.5 Å^{-1}). The main Fourier peaks are labeled I, II and III. There are clear differences in amplitude and position of these peaks between the S_0 and S_1 states. The peak labeled II is from Mn-Mn interactions at ~2.7 Å.

Figure 7. The contour plot shows the fit-quality-parameter ε^2 for the S_0 state plotted versus the number of the two Mn-Mn interactions. The dashed lines shows the distinct minimum at one Mn-Mn vector at 2.85 Å and two Mn-Mn vectors at 2.7 Å.

Figure 8. Structural models for the Mn cluster with three di-μ-oxo bridged Mn moieties. Options G, I, and J are from DeRose et al., 1994, and L and M are two other viable options. One or two mono-μ-oxo bridged motifs are also present in Options G, I, L, and M. No such motif exists in option J.

Figure 9. Left panel. Fourier transforms of k^3-weighted Sr-EXAFS from oriented Sr-PS II samples at two angles (θ). The dichroism is most readily apparent in Fourier peak II (R' = 3.0 Å) which is assigned to backscattering from Mn. Right Panel. The polar plot shows N_{exp} (filled circles) plotted vs the angle of detection, θ. The solid line is the best fit from which we obtain N_{iso} (number of Mn neighbors to Sr) and ϕ, the angle the Mn-Sr vector makes with the membrane normal.

Figure 10. Fourier Transform of Ca EXAFS from Chelex-treated, layered samples with 2 Ca/PS II (k^3-weighted, k = 2.5–10.5 Å^{-1}. The FTs show the presence of a second Fourier peak in the 2Ca/PS II sample that fits to Ca-Mn that is absent in the control sample.

Figure 11. Refined models for the active site of the OEC in Photosystem II. These models combine the finding from oriented Sr-substituted PS II samples with previous results from Mn

EXAFS on oriented PS II samples. These are derived from core structures that have been described in earlier studies (Fig. 11A-B from option A and Fig. 11C from option F in DeRose et al., 1994).
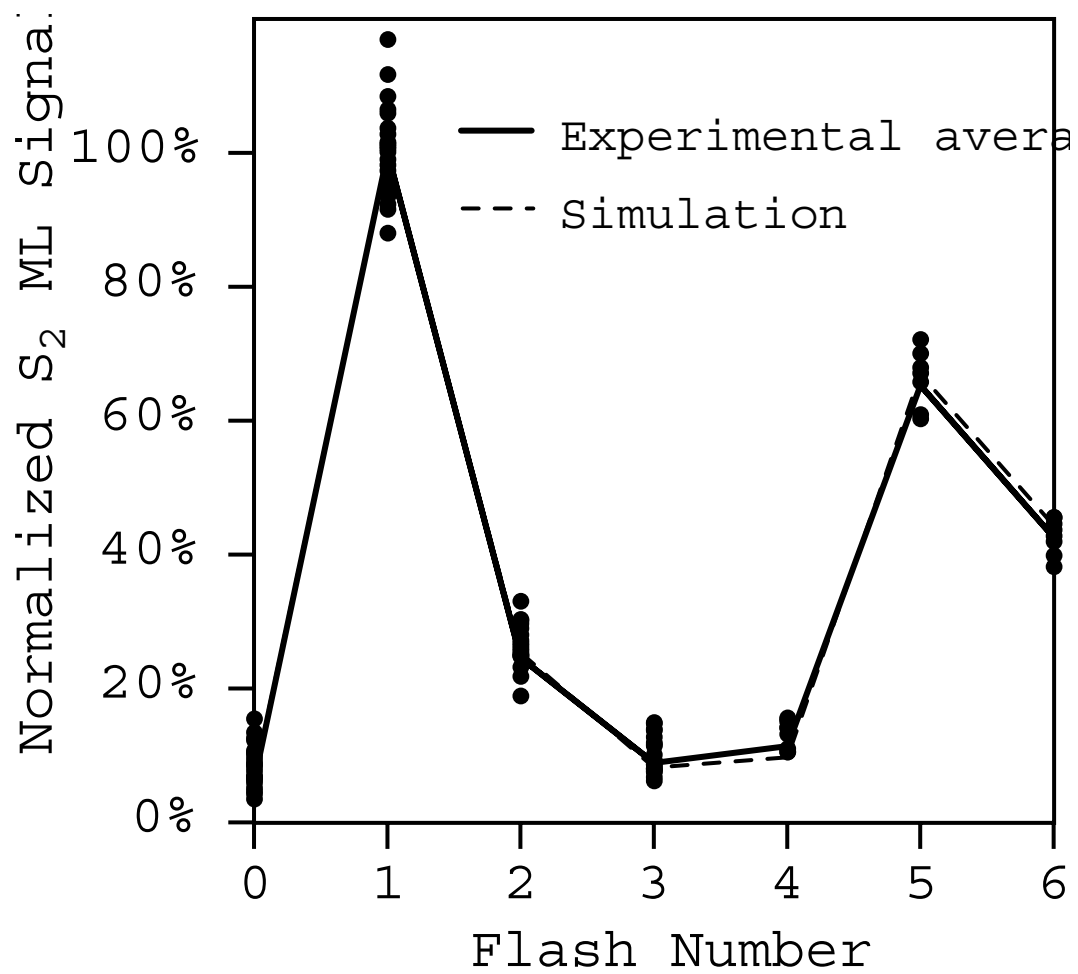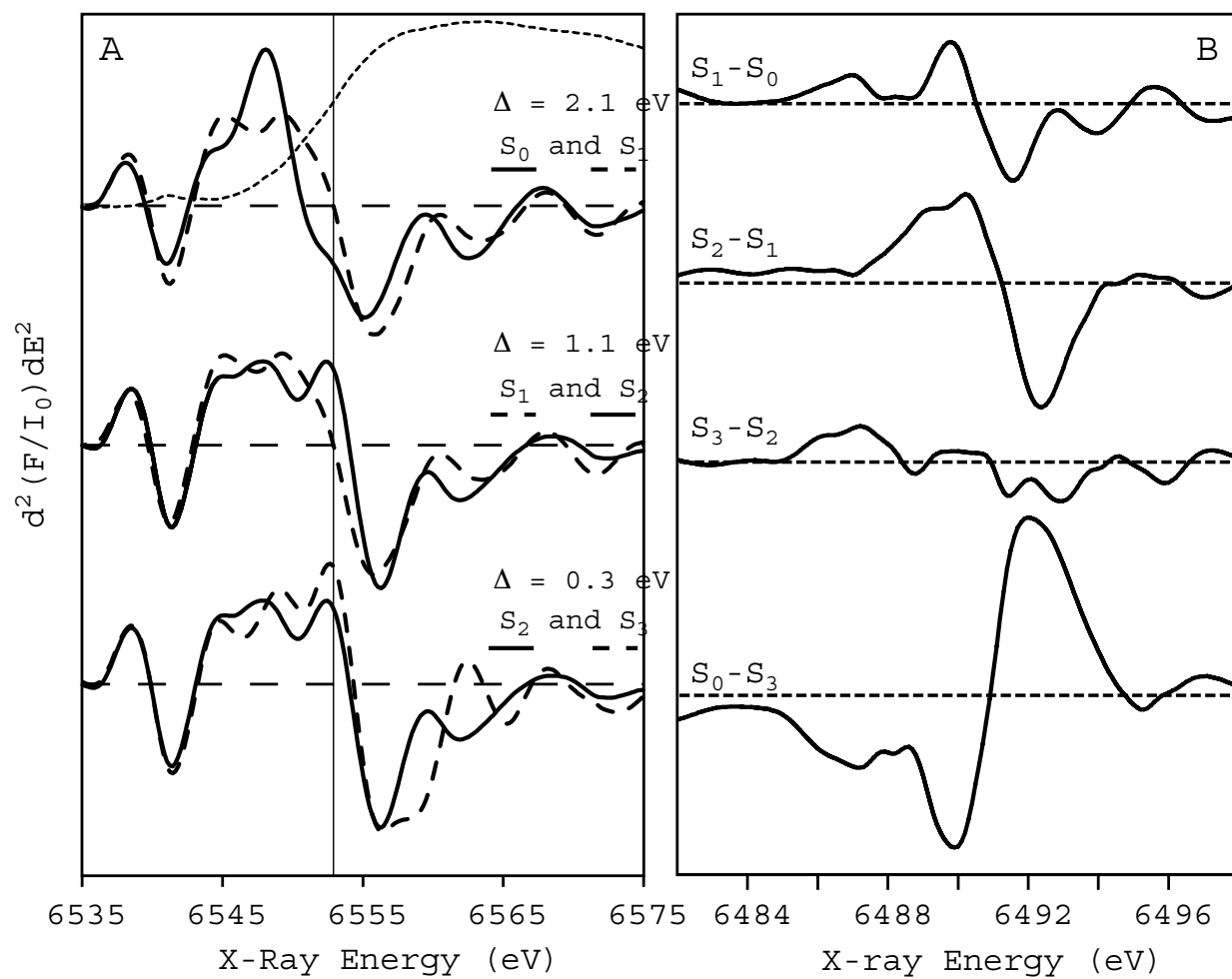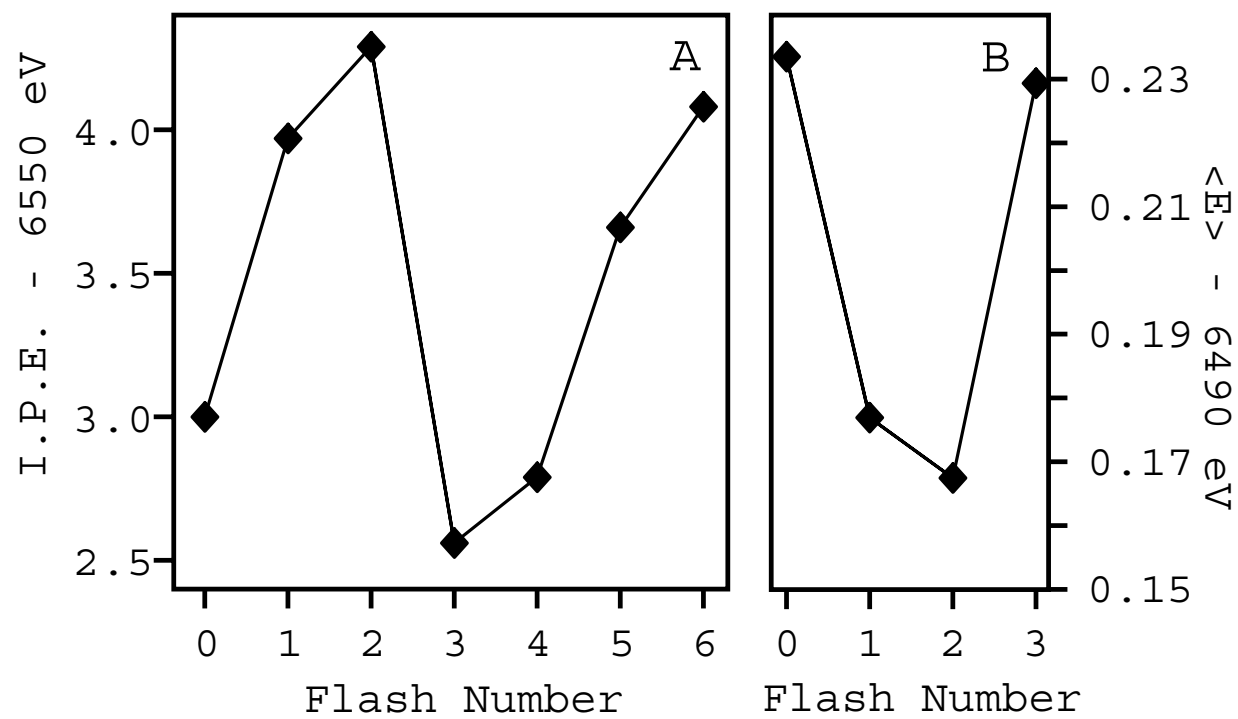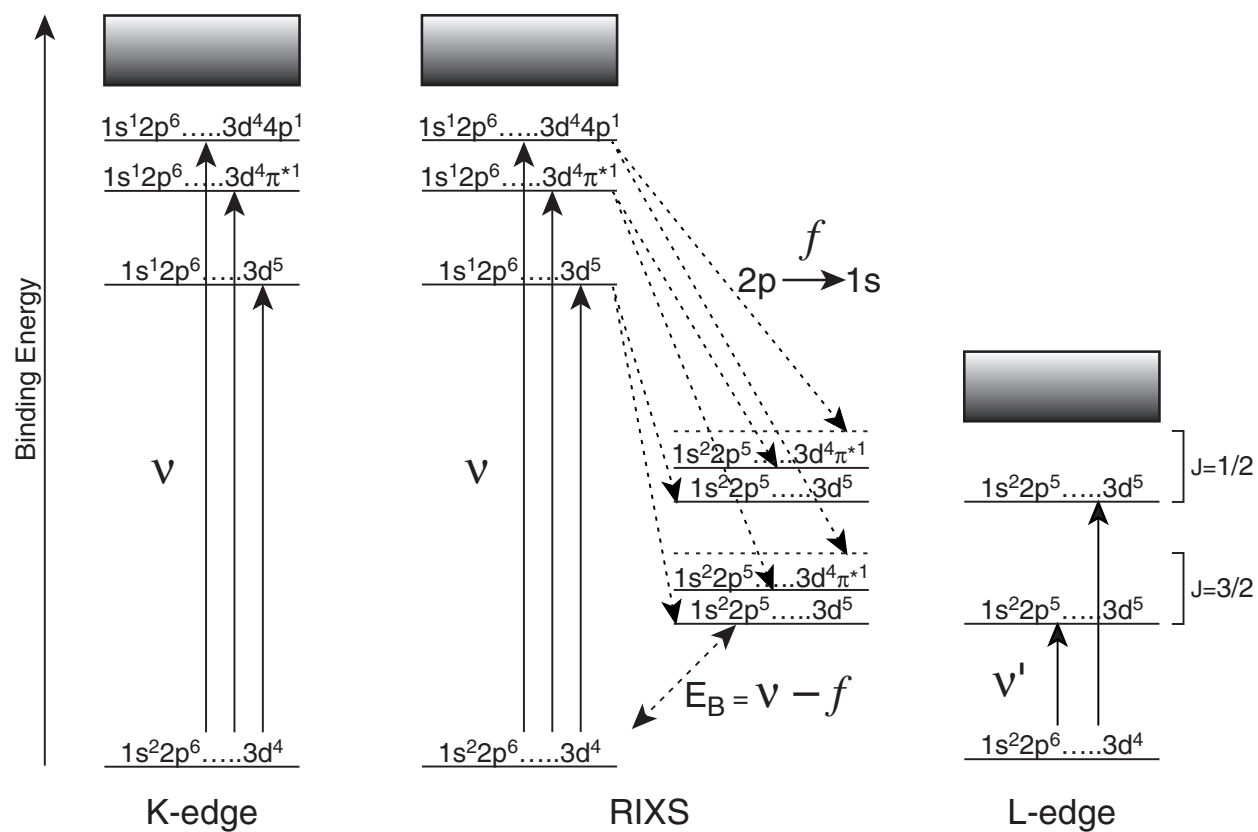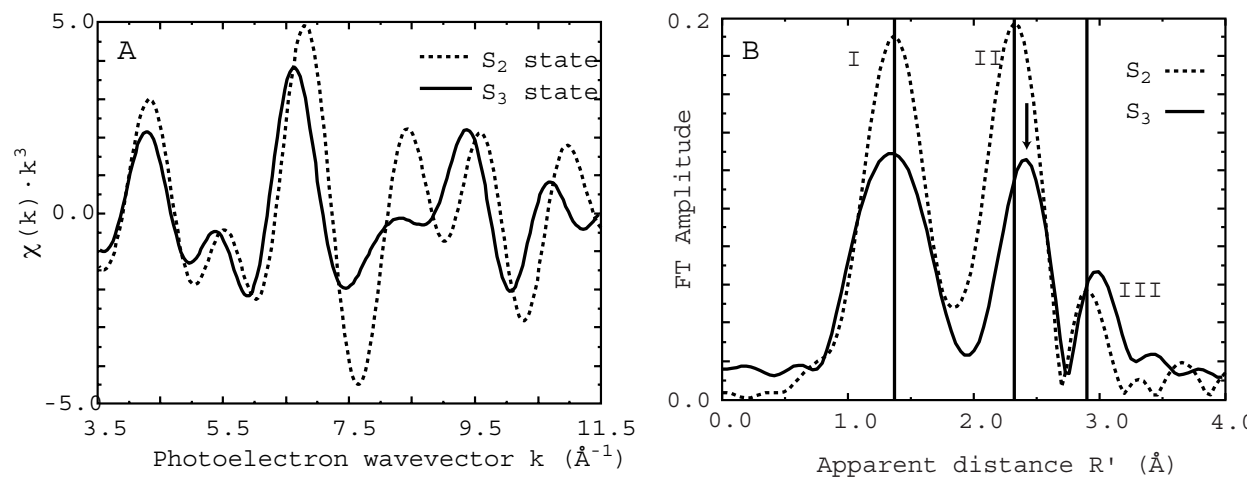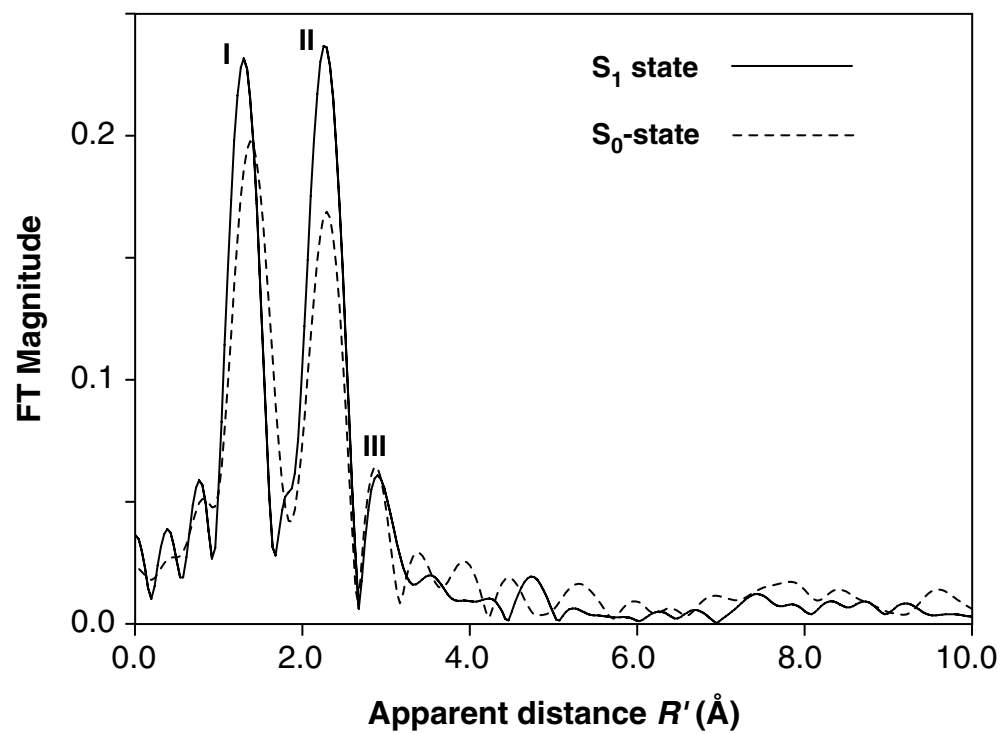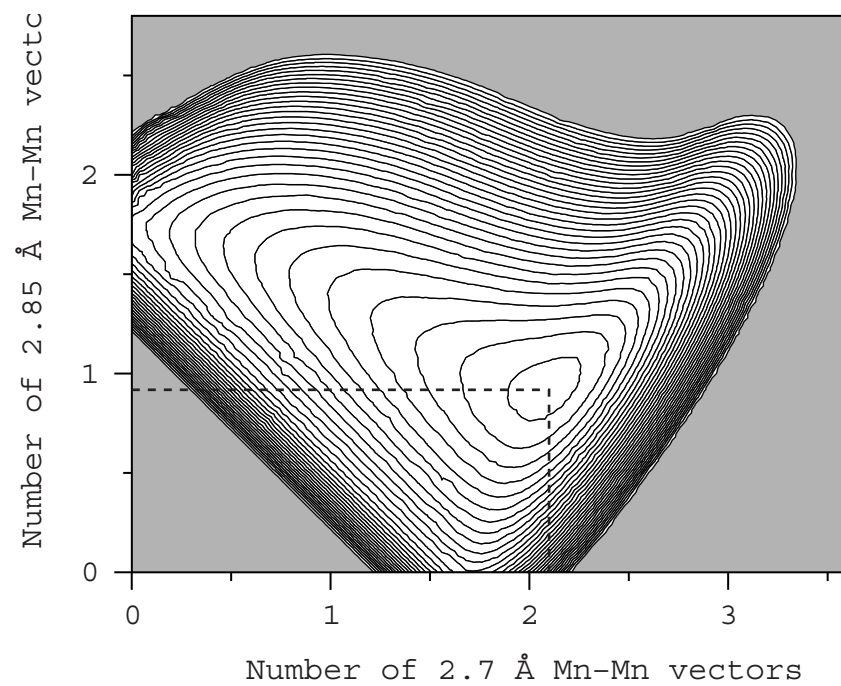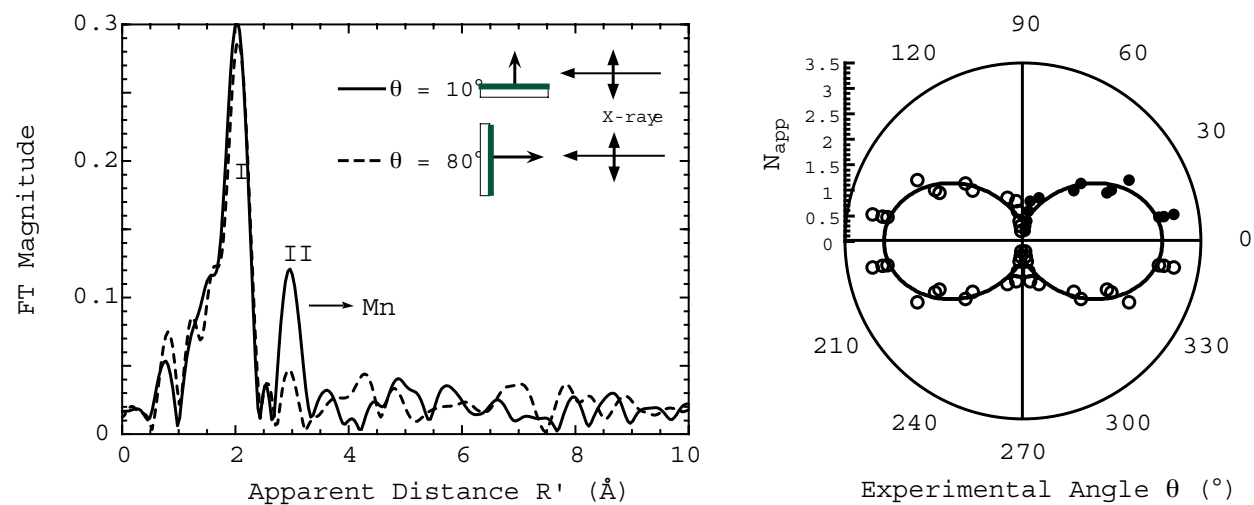
Figure 1

Figure 2

Figure 3

Figure 4

Figure 5

Figure 6

Figure 7
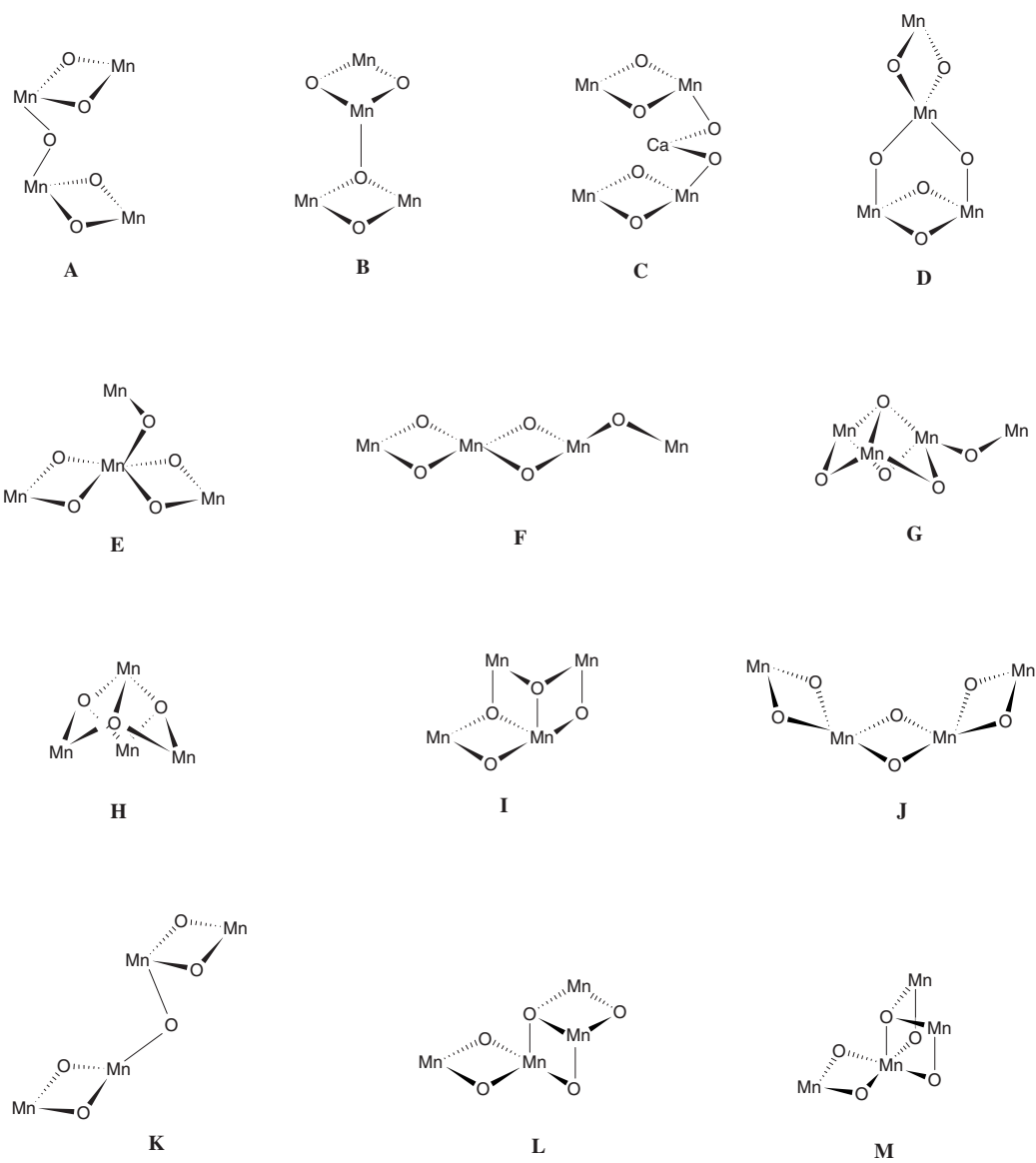
Figure 8

Figure 9

Figure 10

Figure 11